Materials Horizons

ROYAL SOCIETY OF CHEMISTRY

COMMUNICATION

View Article Online
View Journal

Check for updates

Cite this: DOI: 10.1039/d5mh02428e

Received 21st December 2025,
Accepted 18th May 2026

DOI: 10.1039/d5mh02428e

rsc.li/materials-horizons

Ice sliding on nanoscale-smooth surfaces and the role of the quasi-liquid layer

Federica Marelli,[a] Luca Stendardo,[a] Matteo Pedroni,[b] Espedito Vassallo,[b] Samuele Tosatti,[c] Aleksandra Cebrat,[c] Kevin Golovin,[d] Carlo Antonini*[a] and Irene Tagliaro[a]

Understanding ice adhesion and detachment from solid surfaces is essential for the rational design of effective icephobic coatings. In this study, we present a peculiar regime of ice sliding on surfaces with a roughness in the nanometer range, demonstrating that sliding can be consistently observed on various surfaces, including glass and polysaccharide-based monolayer coatings. Such sliding can be interpreted as the macroscopic manifestation of an interfacial layer, often referred to as quasi-liquid layer or pre-molten layer. To test the hypothesis, ice sliding experiments were conducted at different pushing speeds, roughness values and temperatures, on bare and coated glass, providing information on the nanoscale surface properties and behavior of ice at the interface. As such, we pave the way to the rational design of nanoscale-smooth surfaces and materials, that take advantage of interfacial quasi-liquid layer to reduce ice adhesion. Also, polysaccharides are non-toxic and biodegradable, properties that make them suitable as sustainable environmental-friendly coatings.

New concepts

Understanding the behaviour of ice on solid surfaces is relevant both from a fundamental perspective and for the rational design of icephobic materials and surfaces. One of the major debated questions is the existence of a quasi-liquid layer at the ice–solid substrate interface, similarly to the one observed at ice–air interfaces. In this study we investigate ice sliding on nano-scale smooth surfaces, identify the dependence of the mechanism upon temperature and discuss how these results can be interpreted as a macroscopic manifestation of the interface ice properties, providing indirect evidence of a quasi-liquid layer at the ice–solid substrate interface. Specifically, tuning nano-scale roughness allows an estimation of the quasi-liqiud layer as function of temperature. Specifically, we demonstrate ice sliding on polysaccharide transparent nanofilms, namely hyaluronic acid and chitosan. As such, we pave the way to the rational design of nanoscale-smooth materials and surfaces, that take advantage of interfacial quasi-liquid layer to reduce ice adhesion. Also, polysaccharides are non-toxic and biodegradable, properties that make them suitable as sustainable environmental-friendly coatings.

1. Introduction

Ice formation and accretion on solid surfaces, such as wind turbines, solar panels and aircrafts,[1] has a major impact on system operation and human safety. Tackling the problem requires a correct understanding of ice adhesion on surfaces, which can help to design different classes of materials to mitigate icing.[2] The most investigated are hydrophobic surfaces,[3–7] with the underlying assumption that hydrophobicity may promote icephobicity, even if this does not always apply.[8–14] On the opposite side of the wetting spectrum, hydrophilic surfaces are also attracting attention to control ice adhesion.[15,16] In this case, it has been suggested that the strong interactions, such as hydrogen bonds (H-bonds), between a hydrophilic surface and water molecules can influence ice properties at the interface.[17] Indeed, both calculations and experimental tests performed by X-ray diffraction and absorption, or ellipsometry,[18] customized attenuated total reflectance (ATR) techniques[19] and laser confocal microscopy combined with differential interference contrast microscopy (LCM-DIM)[20] confirm the formation of a quasi-liquid layer (QLL), also called pre-molten layer, on free surfaces,[19,21] including the surface of ice.[20,22–26] On the ice surface, the QLL is a state of water 20 to 200 times more viscous than liquid water,[20] with a thickness in the nanometer range that decreases with decreasing temperature.[19,26–28] In the case of ice–solid interfaces, the presence of such QLL would affect ice adhesion, in particular promoting ice sliding and easy removal, especially when surface roughness is of the same order of magnitude.[29] The experimental investigation of the QLL on ice–solid interfaces is very challenging when in presence of high amounts of water

---

[a] Department of Materials Science, University of Milano-Bicocca, 20125 Milan, Italy. E-mail: carlo.antonini@unimib.it
[b] Institute for Plasma Science and Technology (ISTP), National Research Council (CNR), Via R. Cozzi 53, 20125 Milan, Italy
[c] SuSoS AG, Lagerstrasse 14, 8600 Dübendorf, Switzerland
[d] Department of Mechanical & Industrial Engineering, University of Toronto, Toronto, ON M5S 3G8, Canada

at relatively high temperatures. By experimental techniques such as scanning tunneling microscopy (STM) or scanning probe microscopy (SPM) in combination with X-ray photoelectron spectroscopy, it has only been possible to characterize monolayer water structures on metal oxides at temperatures around −200 °C. Currently, there are no experimental techniques available to estimate the QLL thickness at ice–solid interfaces. However, controlling QLL characteristics to promote sliding would be scientifically intriguing and desirable for icephobicity applications.

In this study, we systematically investigated ice adhesion on smooth surfaces (including glass and polysaccharide monolayer coatings), where the occurrence of peculiar regimes of ice sliding provides the macroscopic manifestation of the existence of an interfacial layer of quasi-liquid water. Glass was first investigated by varying levels of roughness and temperature, to define in which conditions sliding occurs. Then, polysaccharides were used to further tune the amount of water adsorbed on glass, grafting polysaccharide monolayers through the nitrene-generating, adhesion-promotion polymer, AziGrip4™.[30] Among hydrophilic substances, polysaccharides were chosen for several reasons: (i) due to the presence of several hydrophilic groups (*i.e.* hydroxyl moieties), they are able to interact with many water molecules and to structure water in different water states[17] possibly favoring the formation of a QLL on polysaccharide-based materials; (ii) each polysaccharide can establish different interactions with water depending on its chemical structure, altering the water states at the interface; (iii) polysaccharides have been already studied to fabricate surfaces with reduced ice adhesion,[31–33] and a QLL[34] has been postulated; (iv) polysaccharides are non-toxic and biodegradable, making them suitable as possible coatings in real applications.[17] Sliding experiments conducted at different pushing speeds, roughness values and temperatures helped to confirm nanoscale surface properties and behavior of ice at the interface.

2. Results and discussion

Our investigation began with the study of ice detachment behavior on glass by varying different parameters and conditions. Ice adhesion measurements were performed on a custom-built horizontal push test instrument[35] (Fig. 1(a)), that allows to record the applied force over time. From the force *vs.* time curves, ice adhesion strength (τ) can be derived as $\tau = F/A$, where F is the maximum force recorded, and A is the contact area between the ice block and the sample. Additional details can be found in materials and methods section.

Two different detachment behaviors were identified by performing ice adhesion tests on the samples. The first one was the instantaneous, brittle detachment of ice from the sample. In this case, the recorded force increased linearly with time after the force probe came into contact with ice, and then suddenly decreased to zero when the ice block detached from the surface (Fig. 1(b)). This detachment behavior is the most commonly observed regime, typical of hard materials such as metallic surfaces.[35] The second detachment behavior was ice sliding on the sample. In this case, after a small initial linear increase in force over time, a plateau was reached, which corresponds to the force needed to slide the ice block on the sample surface (Fig. 1(c)); detachment did not occur. This behavior has been rarely observed only on silica-based substrates,[29,36] or on lubricated soft materials.[37]

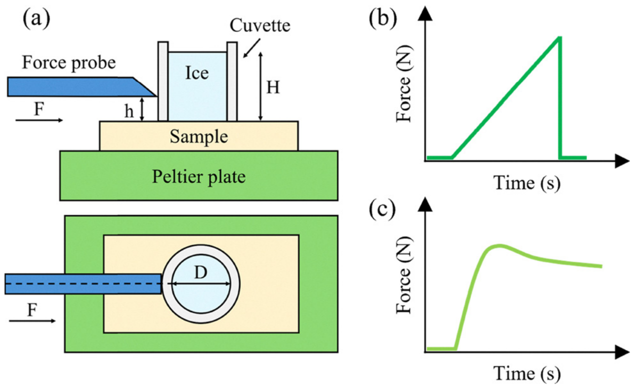

Fig. 1 (a) Schematic representation of the custom-built horizontal shear test setup used to perform ice adhesion measurements (side and top view). Schematic force *vs.* time curves of ice adhesion measurements. Identification of two types of ice detachment regimes: (b) brittle detachment and (c) sliding.

For explaining the occurrence of ice sliding, three hypotheses can in principle be considered: (i) the presence of a liquid lubricating layer, (ii) a solid–solid interaction, with continuous ice-substrate attachment and detachment, and (iii) an intermediate behavior, where the ice close to the interface displays liquid–solid (plastic) behavior, *i.e.* in the presence of the so called QLL. As such, a systematic study was conducted, in which the pushing speed, surface roughness and the surface temperature were changed, thereby validating one of the three hypotheses.

The effect of pushing speed was investigated on standard microscope glass slides (see Fig. S1 in SI). At −6 °C from 0.005 mm s^{-1} up to 0.08 mm s^{-1}, the sliding of ice on glass was always observed at $\tau \sim 400$ kPa, while at 0.16 mm s^{-1} brittle detachment of the ice block occurred at $\tau = 705 \pm 64$ kPa. Similarly, at −9 °C, sliding was observed from 0.005 mm s^{-1} up to 0.04 mm s^{-1} at $\tau \sim 700$ kPa, while brittle detachment happened instead at $\tau = 1002 \pm 36$ kPa at a pushing speed of 0.08 mm s^{-1}. The results show that, in the ice sliding regime, there is no statistically significant dependence of τ on the pushing speed; τ only depends on temperature, even for pushing speed varying by one order of magnitude. This provides evidence against the hypothesis of pure liquid lubrication. Indeed, one may consider that for a shear rate $\dot{\gamma} = V/h \approx 10^{-2}$ mm s^{-1}/10 nm = 10^{3} s^{-1}, where V is the speed and h the lubricant thickness, an effective viscosity could be estimated of the order of $\mu_{\text{QLL}} = \tau/\dot{\gamma} \approx 10^{2}$ Pa s. However, for a Newtonian fluid the force would scale linearly with velocity as $F \propto \mu_{\text{QLL}} V/h$, while our experiments clearly show that the force is constant with increasing velocity. As such, the above scaling would be preserved only if h scaled with velocity, increasing by an order of magnitude, which is unlikely. Among non-Newtonian fluids, yield-like fluids show a yield strength, $\tau = \tau_0 + C\dot{\gamma}^m$, where τ_0 is the yield stress, C is a material constant, $\dot{\gamma}$ is the shear rate, and $m \neq 0$ is the sensitivity index. Our data would indicate that $m = 0$, behavior characteristically different from other yield-like fluids.

Also, sliding is observed up to a maximum speed of 0.08 mm s^{-1} at −6 °C or 0.04 mm s^{-1} at −9 °C, above which brittle detachment is observed. As such, from preliminary analysis on glass, the first hypothesis of lubricant liquid layer can be excluded.

2.1. Effect of surface roughness

Glass slides characterized by different surface roughness values were prepared (see materials and methods section for more details regarding preparation procedure) and tested to assess the ice detachment behavior. The chosen surfaces have roughness, S_a, ∼1 nm (the same standard microscope glass slides used to study the effect of pushing speed; Fig. 2(a)), ∼6 nm (Fig. 2(b)), ∼7 nm (Fig. 2(c)) and ∼16 nm (Fig. 2(d)). By performing ice adhesion tests it was observed that, by increasing the roughness from ∼1 nm to ∼16 nm, an increase in ice adhesion strength occurred from ∼400 kPa to ∼700 kPa at the highest temperature (−6 °C), and from ∼800 kPa to ∼2000 kPa at the lowest temperature (−15 °C) (Fig. 2(e)). In general, by increasing roughness, higher ice adhesion strength values were recorded in the whole temperature range, and a steeper increase in τ was observed for the roughest samples. In addition, for each roughness, a change in the ice detachment regime was observed at different temperatures: at −6 °C ice slides at each roughness (closed symbols, Fig. 2(e)), whereas at −15 °C brittle detachment occurred instead (open symbols, Fig. 2(e)). At intermediate temperatures (−9 °C and −12 °C), mixed behavior was observed (half symbols, Fig. 2(e)). The transition temperature from sliding to brittle detachment increased at higher roughness.

In the hypothesis of a solid–solid interaction with continuous ice-substrate attachment and detachment, we would expect a consistent increase in ice adhesion strength at increased roughness across all temperatures, because of the increased ice-substrate effective contact area. However, the dependence on roughness is not consistent, as three out of four samples exhibited the same ice adhesion strength at −6 °C, and different values at lower temperatures: this trend cannot be explained using the second hypothesis of a solid–solid interaction with continuous ice-substrate attachment and detachment.

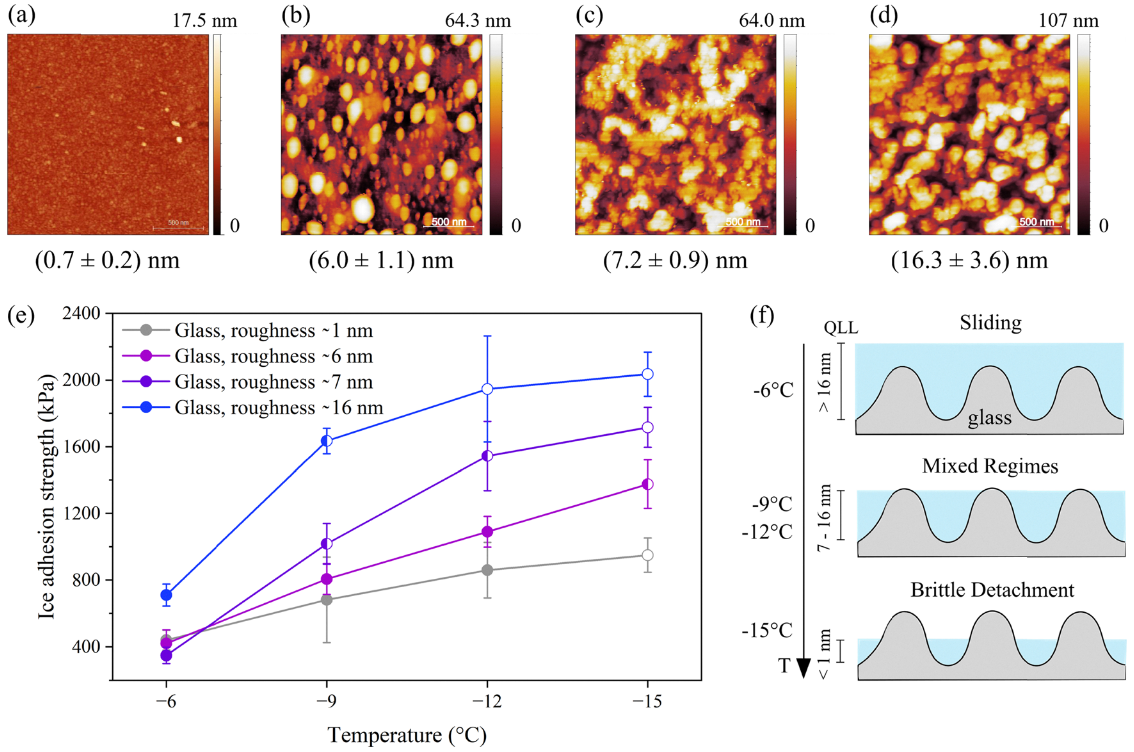

Fig. 2 AFM measurements (scale bar = 500 nm) and mean roughness (S_a, average of three measurements) of glass substrates with different roughness: (a) ∼1 nm, (b) ∼6 nm, (c) ∼7 nm and (d) ∼16 nm. (e) Ice adhesion strength on glass with different roughness: ∼1 nm (grey line), ∼6 nm (fuchsia line), ∼7 nm (purple line) and ∼16 nm (blue line), at −6, −9, −12 and −15 °C; open symbols indicate brittle detachment, while half symbols indicate a mixed behavior. Ice adhesion strength was calculated as F/A (where F is the maximum force of the curve and A the contact area between ice and sample) for both sliding and brittle detachment (average of three measurements). (f) Schematic representation of the dependence of the detachment regime on roughness and QLL: when the QLL thickness is greater than the roughness ice slides on glass (top); when the QLL thickness and roughness are comparable, a mixed behavior is observed (middle); when the QLL thickness is below the roughness level, brittle detachment happens (bottom).

Alternatively, the presence of a QLL can explain why ice adhesion strength and detachment behavior vary according to surface roughness and temperature. According to this hypothesis, sliding can happen only if the QLL thickness exceeds the morphological features generated by roughness (Fig. 2(f)).[38] Thus, when the thickness of the QLL exceeds the roughness, sliding is observed. In contrast, when the QLL thickness is smaller than the roughness, brittle detachment occurs, due to mechanical interlocking between the ice and surface roughness features.

Based on the experimental data presented above, it is possible to infer the QLL thickness at different temperatures, considering that the QLL thickness reduces by reducing temperature.[18] At −6 °C, ice slides at all roughness values up to S_a ∼16 nm, suggesting a QLL thickness >16 nm. At −9 and −12 °C, we observed ice sliding on all surfaces with roughness values up to S_a ∼7 and 16 nm, where an intermediate behavior occurs. As such, at these temperatures we can infer a QLL thickness in the range between 7 and 16 nm. At −15 °C, since no sliding is observed even on the smoothest sample, the QLL thickness is <1 nm. This trend is in good agreement with experimental studies performed with glancing-angle X-ray scattering.[39]

Therefore, the dependence of τ upon temperature can be interpreted as a macroscopic manifestation of the interface ice properties. These results are in agreement with recent studies[40] that investigated ice sliding by molecular dynamic (MD) simulations and identified that heat and pressure do not cause melting. Instead, it has been reported that a displacement-driven amorphization occurs, which becomes more significant at temperatures near 0 °C. This mechanism is explained by structural breakdown and plastic deformations happening during sliding, which can fall under the third hypothesis stated above. It has been reported that temperature can affect two QLL properties: viscosity and thickness. By reducing the temperature, an increase in equivalent viscosity makes sliding more difficult. This is also in agreement with the definition of QLL,[29,36] which is more viscous than liquid water[20] due to stronger H-bonds.[24] Moreover, since the QLL thickness decreases upon temperature reduction,[19,26–28,41] the force needed for sliding increases, leading to a gradual increase of τ and finally to a brittle detachment instead of sliding.[29]

2.2. Effect of surface chemistry

For evaluating the effect on surface chemistry on ice adhesion, we coated standard microscope glass slides with S_a ∼1 nm, corresponding to the samples that displayed the best performance during the previous investigations. Two types of polysaccharides were chosen to tune the surface chemistry because of their water-binding properties, which make them good candidates for increasing water-substrate interactions. Thin films were deposited ensuring a good morphological conformation of the coating with the substrate in terms of roughness.

Polysaccharide monolayers were obtained as shown in Fig. 3(a)–(f), using the adhesion–promotion polymer, AziGrip4™, to link the polysaccharide chains to the glass substrate.

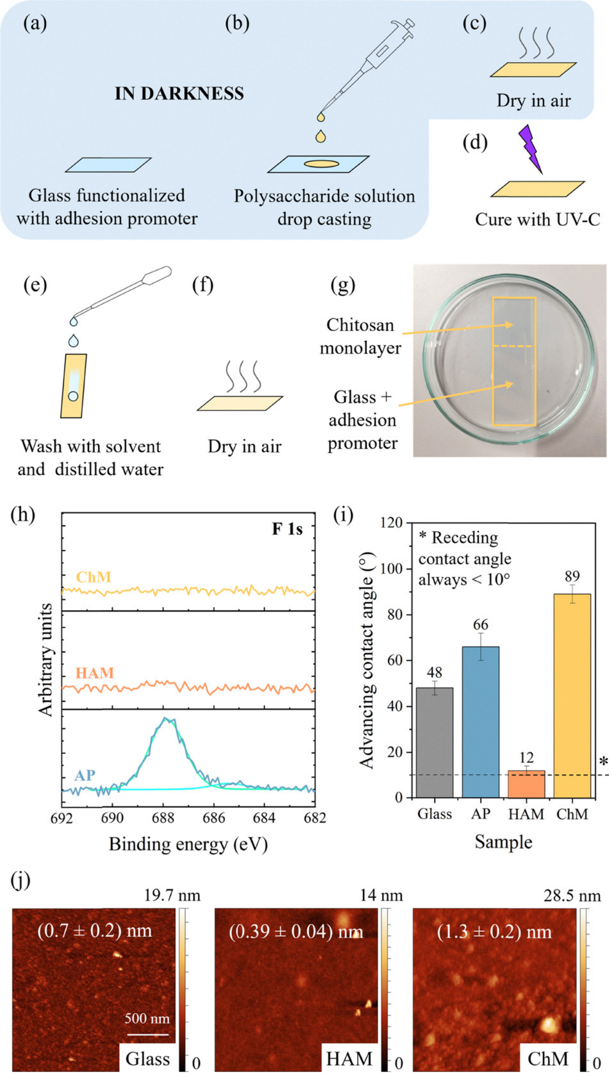

Fig. 3 (a) Schematic representation of the polysaccharide monolayers preparation: (a) glass slide already functionalized with the adhesion promoter; (b) drop casting of polysaccharide solution; (c) solvent evaporation; these three steps were performed in darkness, to avoid adhesion promoter degradation; (d) UV-C curing; (e) washing with solvent and distilled water to remove excess of polysaccharide; (f) monolayer ready for testing. (g) Picture of a glass slide only partially covered with a chitosan monolayer, showing its complete transparency. (h) XPS spectra of F 1s region confirm the successful polysaccharide layers deposition with the attenuation of fluorine signal from underlaying adhesion promoter. (i) Water advancing contact angles of glass (grey column), glass functionalized with the adhesion promoter (AP, light blue column), hyaluronic acid monolayer (HAM, orange column) and chitosan monolayer (ChM, yellow column) (average of four measurements); receding contact angles always <10° (not shown for simplicity). (j) AFM measurements (scale bar = 500 nm) and mean roughness (S_a, average of three measurements) of glass, hyaluronic acid monolayer (HAM) and chitosan monolayer (ChM). Adhesion promoter (AP) coated sample roughness is the same as glass.

This adhesion promoter contains a polymer backbone composed of repeating aliphatic amine units grafted with fluorinated phenyl rings containing azide groups, inducing covalent bonds with the polysaccharide *via* C–H and/or N–H insertion reactions that are activated by either UV-light or temperature to form highly reactive nitrene groups.[30,42] The obtained polysaccharide monolayers were visually transparent (Fig. 3(g)). See materials and methods section for more details regarding samples preparation.

X-ray photoelectron spectroscopy (XPS) measurements confirmed the presence of the adhesion promoter on glass (AP) as well as the successful deposition of hyaluronic acid and chitosan grafted layers (Fig. 3(h)). The characteristic fluorine signal in F 1s region originating from the adhesion promoter is clearly visible on the pretreated glass samples. Upon deposition of the polysaccharide layers, the fluorine signal was completely attenuated, indicating full coverage of the promoter layer (see also Fig. S2(a) in SI for C 1s spectra). The thickness of the polysaccharide layers, namely hyaluronic acid monolayers (HAM) and chitosan monolayers (ChM), was also estimated to be less than 10 nm (Fig. S2(b) in SI). Since the probe depth of XPS is maximum ∼10 nm and in our data we can still observe the Si 2s and 2p signals, which are located at the lowest part of the coating system, we can conclude that the coating is less than 10 nm thick. The fact that this type of approach results in a single polymer layer has been already described in the paper of Serano *et al.*[43] for other polymers and a similar adhesion promoting system.

Advancing contact angles of the four samples were also significantly different from each other (Fig. 3(i) and Fig. S3 in SI), confirming effective surface modification. HAM (advancing contact angle, θ_A = 12°) were the most hydrophilic samples, while ChM were the most hydrophobic (θ_A = 89°). As a reference, glass (θ_A = 48°) and glass covered by the adhesion promoter (AP, θ_A = 66°) exhibited intermediate wetting behavior, with AP slightly more hydrophobic due to the presence of fluorine atoms, known for their hydrophobicity.[44,45] Receding contact angles were comparable, being lower than 10° for all samples (Fig. S3 in SI). Atomic force macroscopy (AFM) measurements confirmed that roughness of the glass substrate was not significantly altered by the polysaccharide coatings (Fig. 3(j); AP roughness (not shown) was the same as glass[42]). A slight increase in S_a is observed in the case of ChM (1.3 nm ± 0.2 nm), while a small decrease is visible in the case of HAM (0.39 nm ± 0.04 nm) in comparison to AP and glass (0.7 nm ± 0.2 nm).

The coated samples were then tested for ice adhesion at different temperatures, to evaluate the influence of surface chemistry. Fig. 4 shows the results obtained by performing ice adhesion tests on glass, AP, HAM and ChM at different temperatures, namely −6 (Fig. 4(a)), −9 (Fig. 4(b)), −12 (Fig. 4(c)) and −15 °C (Fig. 4(d)). For these tests, the pushing speed was set at 0.01 mm s^{-1}. Over the whole temperature range, glass and AP displayed similar behaviors (see also Fig. 4(e)): ice sliding was observed down to −12 °C, but brittle detachment occured at −15 °C, in agreement with previous results.[29] For polysaccharides, chitosan exhibited the largest ice sliding force at −6 °C (Fig. 4(a)), and at −9 °C brittle detachment was observed. For this reason, no further tests were performed for chitosan at lower temperatures. Differently, hyaluronic acid was found to significantly reduce the ice adhesion strength of bare glass at −6 °C, with corresponding τ = 79 ± 40 kPa. However, at the lowest tested temperature (−12 and −15 °C), the HAM performance was worse than that of glass, suggesting a higher impact of temperature on HAM with respect to glass.

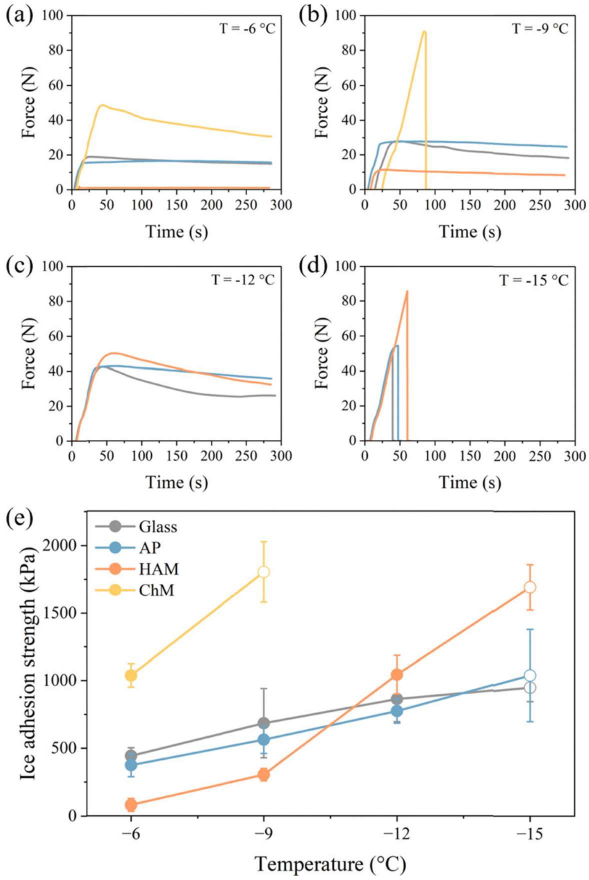

Fig. 4 Representative force profiles recorded during ice adhesion measurements at (a) −6 °C, (b) −9 °C, (c) −12 °C and (d) −15 °C, for glass (grey line), glass functionalized with the adhesion promoter (light blue line), hyaluronic acid monolayer (orange line) and chitosan monolayer (yellow line). Pushing speed = 0.01 mm s^{-1}. (e) Ice adhesion strength on glass (grey line), glass coated with the adhesion promoter (AP; light blue line), hyaluronic acid monolayer (HAM; orange line) and chitosan monolayer (ChM; yellow line), at −6, −9, −12 and −15 °C; closed symbols indicate sliding while open symbols brittle detachment. Ice adhesion strength was calculated as *F*/*A* (where *F* is the maximum force of the curve and *A* the contact area between ice and sample) for both sliding and brittle detachment (average of four measurements).

To explain these trends, we refer to the above-mentioned dependence of the QLL on the surfaces' wetting properties: an increase in hydrophilicity increases QLL thickness due to the establishment of stronger intermolecular interactions between water and surface, reducing τ.[41] Also in the case of coated substrates, our results agree with these observations. Down to −9 °C (Fig. 4(e)), the roughest and most hydrophobic sample (ChM) showed the highest τ, whereas the smoothest and most hydrophilic material (HAM, see also Fig. 4(e)), showed the lowest τ. In the case of smoothest samples (glass, AP and HAM), we observe a regime transition to brittle detachment at −15 °C, resulting in a QLL estimated thickness <1 nm.

In the case of ChM, we speculate that, due to increase in hydrophobicity, the QLL thickness shrinks to <1 nm at higher temperatures, already at -9 °C.

We have also verified that differences in molecular weight do not significantly influence ice adhesion in the case of chitosan (see Fig. S4 in SI for a comparison between two chitosan coatings, with low and high molecular weight, showing comparable results).

To evaluate the durability of the polysaccharide coatings, we repeated multiple ice adhesion measurements on the same sample (Fig. S5) and confirmed by XPS the persistence of the coating (Fig. S1(a)).

Interestingly, polysaccharide monolayers showed stronger variations in τ as function of temperature compared to pristine glass and AP (Fig. 4(e)). This behavior may suggest a strong influence of the coating chemistry on QLL characteristics. Both polysaccharides and glass surfaces bear hydroxyl groups able to establish H-bonds with water molecules. However, the presence of long polysaccharide chains greatly increases the number of hydroxyl groups available to interact with water, especially for hydrophilic hyaluronic acid (see contact angles, Fig. 3(i)). While specific MD simulations would be prohibitive due to the high computational resources required for the high molecular weight polysaccharides tested here, speculative hypothesis can be brought into the discussion. Hyaluronic acid is known for its lubricating properties and ability to bind many water molecules,[46,47] thanks to its flexible conformation[48] combined with favorable functional groups orientation for H-bonds. If compared to the rigid surface of glass, the increased flexibility of the OH interface can likely arrange an increased number of H-bonds geometrically oriented for maximizing proton donor and proton acceptor alignment.[49,50] Moreover, hyaluronic acid was found to act as a structure maker to increase water molecules order. Indeed, near-IR spectroscopic investigations proved that low concentrations of hyaluronic acid may promote the conversion of weaky-bound water states into strongly hydrogen bonded water species.[51] This may promote the formation of a thicker QLL on HAM, which is an advantage at temperatures closer to 0 °C, facilitating sliding. However, as temperature decreases, the ice resistance to sliding sharply increases to values higher than those on glass. This observation may be due to the presence of many water–polysaccharide interactions, that increase the strength of the ice–polysaccharide interactions, making it more difficult to displace or detach ice from HAM than glass. The ChM results suggest a similar trend compared to HAM. However, chitosan structure favors intramolecular H-bonds, promoting a more rigid and elongated chain conformation[48] that hinders the exposure of functional groups able to interact with water, which causes higher resistance to sliding on ChM even at temperatures closer to 0 °C (specifically, -6 °C), leading to brittle fracture already at -9 °C. Our hypothesis is that the complex polysaccharide-water interactions affected by polysaccharide conformation and the availability of OH groups may result in a difference in the temperature dependance of the ice adhesion strength.

3. Conclusions

To summarize, we have investigated the effect on ice adhesion properties of different substrate parameters including roughness, temperature and chemical modification on bare and coated glass. Beside a standard brittle detachment mode, our experiments evidenced the occurrence of a rarely reported sliding effect, particularly persistent at low surface roughness, high temperature and on more hydrophilic substrates. The observation of this peculiar regime and its dependency on temperature is in agreement with the existence of a QLL, also known as pre-molten layer, at the ice-substrate interface. As expected, smooth glass samples provided the lowest ice adhesion at all temperatures analyzed (from -6 to -15 °C), due to a reduced interlocking mechanism occurring with ice. A thin hyaluronic acid coating was found to significantly reduce the ice adhesion strength at -6 °C, with corresponding $\tau = 79 \pm 40$ kPa. All polysaccharide coatings show increased temperature dependence in comparison with glass due to more complex ice-substrate interactions. Moreover, our findings provide an indirect experimental evaluation of QLL thickness by observation of ice detachment modes on substrates of defined roughness. Based on our experiments, we have estimated that the QLL thickness at the ice-substrate interface is >16 nm at -6 °C, while it shrinks to <1 nm at -15 °C.

We envision that the findings presented in this work can pave the way for further studies on the QLL on nanoscale-smooth surfaces, so that its thickness can be eventually tuned based on the material choice. Some experimental techniques such as AFM-IR and laser confocal microscopy combined with differential interference contrast microscopy[20] can help to capture water and ice behavior in the presence of complex macromolecules on a solid surface. In addition, with increased computational power, MD simulations will further shed light on this phenomenon.

4. Materials and methods

4.1. Materials

Chitosan 75/500 (200–300 kDa, 75% deacetylation degree, CAS 9012-76-4) and Chitosan 75/20 (50 kDa, 75% deacetylation degree, CAS 9012-76-4) were bought from Heppe Medical Chitosan GmbH. Hyaluronic acid (800 kDa) was kindly supplied by Istituto di Ricerche Chimiche e Biochimiche G. Ronzoni. Acetic acid (glacial, 99+%, CAS 64-19-7) was bought from ThermoFisher (Kandel) GmbH. Standard glass microscope slides were purchased from Colaver s.r.l. (Art. No. 64CE2910, 76 mm × 26 mm × 1 mm) and VWR (Dietikon, Switzerland, Art. No. 631-1550, 76 mm × 26 mm × 1 mm). Distilled water was used throughout the study.

4.2. Glass etching

Glass substrates with different surface roughness were prepared by plasma etching using a CF_4/Ar mixture. In these plasmas, SiO_2 erosion occurs *via* chemical reaction with fluorine radicals ($F^\bullet$), which form volatile SiF_4 species, while ion bombardment (Ar^+ and CF_x^+ ions) physically sputters the surface and removes partially volatile products, introducing anisotropy in the etching process. The nanostructuring of the glass is governed by a self-masking dynamic mechanism, in which clusters of less volatile fluorocarbon compounds are locally deposited. Continuous film formation is inhibited by ion sputtering, so these clusters act as temporary masks that locally protect the surface, leading to the formation of self-organized conical or pillar-like nanostructures. Conventional glass slides, such as soda-lime or borosilicate substrates, contain impurities including Na, Ca, and Al. In contact with fluorine, these elements can form non-volatile compounds that significantly reduce the etch rate and hinder nanostructure formation. For instance, soda-lime glass etched in CF_4/CHF_3 plasma exhibits etch rates of $\sim$4 nm min^{-1}, compared to $\sim$45 nm min^{-1} for impurity-free SiO_2, as reported in the literature.[52] To achieve faster, controlled, and high-aspect-ratio nanostructuring, the glass slides were first coated with a $\sim$1 μm layer of pure SiOx deposited by PECVD. The deposition conditions and chemical characteristics of the SiOx coating are detailed in previous publications.[53] The morphology of the SiOx nanostructures is controlled by the applied bias, CF_4/Ar ratio, chamber pressure, and etching time, which collectively determine the balance between ion sputtering, fluorocarbon polymer deposition, and chemical etching by fluorine radicals. To achieve roughness on the order of tens of nanometers, the following process parameters were used: CF_4/Ar flow rate = 25/5 sccm, pressure = 6 Pa, and bias voltage = 500 V. By varying the etching time, the density and dimensions of the nanostructures can be tuned. The plasma etching apparatus used in this study is described in previous publications.[54]

4.3. Glass slides functionalization

The glass slides were coated with a nitrene-generating adhesion promoter[30] (AziGrip4™ amine, SuSoS AG, Dübendorf, Switzerland) following exposure to oxygen plasma (<0.3 mbar; Diener Electronic Nano, Germany) for 2 min. The plasma-cleaned surfaces were immersed in 0.1 mg mL^{-1} AziGrip4™ amine solution, diluted with a 2 : 3 10 mM 4-(2-hydroxyethyl)piperazine-1-ethane-sulfonic acid (HEPES)/ethanol mixture for 30 min. Both surfaces were then rinsed twice in a 2 : 3 HEPES/ethanol mixture, followed by rinsing in ultrapure water, and finally blow-dried with filtered (0.45 μm) nitrogen gas.

4.4. Polysaccharide monolayers production

To produce polysaccharide monolayers, solutions of the polysaccharides were deposited over the functionalized glass slides by drop-casting using a micropipette. For chitosan monolayers (ChM), 75 mg of polysaccharide solubilized in 4 mL of 5% acetic acid were deposited over each glass slide. For hyaluronic acid monolayers (HAM), 75 mg of polysaccharide solubilized in 5 mL of distilled water were deposited over each glass slide. After total evaporation of the solvent, the samples were cured under UV-C irradiation (15 W, 15 min), to form covalent bonds between the adhesion promoter and the polysaccharide chains. An important precaution is to work in dark conditions until the UV-C curing, because the adhesion promoter is sensible to light, and can be degraded if exposed to it, thus lowering its efficiency. The excess of polysaccharide was then washed away using first the same solvent of the polysaccharide and then distilled water. The obtained monolayers are completely transparent and not distinguishable from a bare glass slide by naked eye.

4.5. X-ray photoelectron spectroscopy measurements

The presence and thickness of the monolayers were assessed by X-ray Photoelectron Spectroscopy using a PhI5000 VersaProbe spectrometer (ULVAC-PHI, INC, at SuSoS AG) equipped with a 180° spherical capacitor energy analyzer and a multi-channel detection system with 16 channels. See SI and the reference therein[55] for further details.

4.6. Contact angle measurements

Wettability was assessed by measuring advancing and receding contact angles using a camera (Fastcam Nova S6, Photron) with backlight illumination and a syringe pump (Harvard Apparatus, Pump 11 Pico Plus Elite). To measure advancing and receding contact angles, the syringe pump was used to infuse and withdraw deionized water with the following procedure: infusion of 3 μL, 3 s delay, infusion of 5 μL (advancing contact angle measurement), withdraw of 8 μL (receding contact angle measurement). Infusion and withdrawal rates were always 10 μL min^{-1}. The images were then analyzed with the software ImageJ (DropSnake plug-in).

4.7. Roughness measurements

Roughness was assessed by AFM under ambient conditions using a Core AFM system (Nanosurf GmbH, Langen, Germany). Dyn190Al cantilevers (nominal force constant 28–75 N m^{-1}, tip radius $\sim$10 nm) were operated in dynamic mode to measure glass samples. The images of monolayers samples were obtained in tapping mode (tip PPP-NCR, from Nanosensors), with 10 nm radius, resonance frequency of $\sim$280 kHz and spring constant of 25–30 N m^{-1}. The acquired topographic images were processed and analyzed with Gwyddion software.

4.8. Ice adhesion strength measurements

Ice adhesion measurements were performed on a custom-built horizontal shear (or push) test instrument, which included an environmental chamber, a cooling system, a force sensor, and an actuation system.[35] The sample was placed in the environmental chamber with controlled temperature (T_{amb} = 20 °C) and relative humidity (RH $\sim$ 2%) and was then cooled down by Peltier plates with liquid-cooled heat sink. A cylindrical nylon mold, with an inner diameter of 8 mm, was placed on the sample and used to form the ice block. For ice adhesion measurements, the cooling is imparted from the bottom, to control the temperature and ensure that nucleation starts at the sample surface. The temperature at the interface was actively controlled by a PID controller. The substrate was first cooled down to −20 °C, then 250 μL of water was added into the mold. After 15 min of conditioning to ensure complete water freezing, the temperature was changed to the test temperature (−6, −9, −12 or −15 °C, measured on the surface of the sample) and was maintained for another 5 min of conditioning before performing the push-off test. The push-off test applied a force on the outside of the mold, parallel to the sample, at a pushing height of 1 mm. To do this, a force gauge (Mark-10 model M5-20, resolution 0.01 N) equipped with a metallic rod was employed. The force gauge was moved at a constant velocity through a linear displacement system (Newport LTA-HL with Conex-CC Controller). Since the cylindrical mold containing ice is made of a low thermally conductive material, heat transfer through the cylinder can be neglected, allowing full control of ice temperature. For the tests performed at different temperatures on different samples, the pushing speed was set to 0.01 mm s^{-1}, a quasi-static regime where dynamic effects can be excluded. Tests at different pushing speeds (0.005, 0.01, 0.02, 0.04, 0.08 and 0.16 mm s^{-1}) were also performed on glass. The force gauge records the applied force and from the force *vs.* time curves, the ice adhesion strength can be derived as $\tau = F/A$, where F is the maximum force recorded, and A is the contact area between the ice block and the sample.

Author contributions

Federica Marelli: conceptualization, methodology, formal analysis, investigation, writing – original draft, visualization. Luca Stendardo: conceptualization, methodology, writing – review & editing. Matteo Pedroni: investigation, writing – review & editing. Espedito Vassallo: investigation, writing – review & editing. Samuele Tosatti: methodology, writing – review & editing. Aleksandra Cebrat: investigation, formal analysis, writing – review & editing. Kevin Golovin: conceptualization, writing – review & editing. Carlo Antonini: conceptualization, methodology, formal analysis, writing – original draft, supervision, project administration, funding acquisition. Irene Tagliaro: conceptualization, methodology, formal analysis, supervision, project administration, writing – review & editing.

Conflicts of interest

There are no conflicts of interest to declare.

Data availability

All data generated or analyzed during this study are included in this published article and its supplementary information (SI). Supplementary information includes: (i) effect of pushing speed on ice adhesion; (ii) X-ray photoelectron spectroscopy details; (iii) contact angle measurements; (iv) ice adhesion measurements on chitosan coatings with different molecular weights; and (v) sample durability. See DOI: https://doi.org/10.1039/d5mh02428e.

References cited in the SI have been listed in the article's reference list.

Acknowledgements

The authors are thankful to Michael Thouless (University of Michigan) for suggestions and discussion on results.

References

1 I. V. Roisman, M. Ding, A. Maslov, L. Stendardo and A. R. Shaikh, in *Smart Surface Design for Efficient Ice Protection and Control*, ed. C. Antonini and I. Tagliaro, IOP Publishing, 2025, pp. 1-1–1-58.
2 S. S. Latthe, R. S. Sutar, A. K. Bhosale, S. Nagappan, C.-S. Ha, K. K. Sadasivuni, S. Liu and R. Xing, *Prog. Org. Coat.*, 2019, **137**, 105373.
3 T.-S. Wong, S. H. Kang, S. K. Y. Tang, E. J. Smythe, B. D. Hatton, A. Grinthal and J. Aizenberg, *Nature*, 2011, **477**, 443–447.
4 W. S. Y. Wong, K. I. Hegner, V. Donadei, L. Hauer, A. Naga and D. Vollmer, *Nano Lett.*, 2020, **20**, 8508–8515.
5 Y. Shen, X. Wu, J. Tao, C. Zhu, Y. Lai and Z. Chen, *Prog. Mater. Sci.*, 2019, **103**, 509–557.
6 P. Irajizad, S. Nazifi and H. Ghasemi, *Adv. Colloid Interface Sci.*, 2019, **269**, 203–218.
7 H. Sojoudi, G. H. McKinley and K. K. Gleason, *Mater. Horiz.*, 2015, **2**, 91–99.
8 S. B. Subramanyam, K. Rykaczewski and K. K. Varanasi, *Langmuir*, 2013, **29**, 13414–13418.
9 K. Rykaczewski, S. Anand, S. B. Subramanyam and K. K. Varanasi, *Langmuir*, 2013, **29**, 5230–5238.
10 K. Golovin, S. P. R. Kobaku, D. H. Lee, E. T. DiLoreto, J. M. Mabry and A. Tuteja, *Sci. Adv.*, 2016, **2**, e1501496.
11 V. Hejazi, K. Sobolev and M. Nosonovsky, *Sci. Rep.*, 2013, **3**, 2194.
12 M. Nosonovsky and V. Hejazi, *ACS Nano*, 2012, **6**, 8488–8491.
13 S. A. Kulinich, S. Farhadi, K. Nose and X. W. Du, *Langmuir*, 2011, **27**, 25–29.
14 J. Chen, J. Liu, M. He, K. Li, D. Cui, Q. Zhang, X. Zeng, Y. Zhang, J. Wang and Y. Song, *Appl. Phys. Lett.*, 2012, **101**, 111603.
15 R. Dou, J. Chen, Y. Zhang, X. Wang, D. Cui, Y. Song, L. Jiang and J. Wang, *ACS Appl. Mater. Interfaces*, 2014, **6**, 6998–7003.
16 J. Chen, R. Dou, D. Cui, Q. Zhang, Y. Zhang, F. Xu, X. Zhou, J. Wang, Y. Song and L. Jiang, *ACS Appl. Mater. Interfaces*, 2013, **5**, 4026–4030.
17 F. Marelli, D. Pontoriero, C. Antonini and I. Tagliaro, *Carbohydr. Polym.*, 2025, **368**, 124138.
18 B. Slater and A. Michaelides, *Nat. Rev. Chem.*, 2019, **3**, 172–188.
19 V. Sadtchenko and G. E. Ewing, *J. Chem. Phys.*, 2002, **116**, 4686–4697.
20 G. Sazaki, K. Murata, H. Asakawa, K. Nagashima, S. Nakatsubo and Y. Furukawa, *J. Cryst. Grow.*, 2022, **597**, 126853.
21 E. Ochshorn and W. Cantrell, *J. Chem. Phys.*, 2008, **128**, 134701.
22 I. A. Ryzhkin and V. F. Petrenko, *Phys. Rev. B: Condens. Matter Mater. Phys.*, 2001, **65**, 012205.
23 R. Rosenberg, *Phys. Today*, 2005, **58**, 50–54.

24 M. A. Sánchez, T. Kling, T. Ishiyama, M.-J. Van Zadel, P. J. Bisson, M. Mezger, M. N. Jochum, J. D. Cyran, W. J. Smit, H. J. Bakker, M. J. Shultz, A. Morita, D. Donadio, Y. Nagata, M. Bonn and E. H. G. Backus, *Proc. Natl. Acad. Sci. U. S. A.*, 2017, **114**, 227–232.

25 J. Shi, M. Fulford, H. Li, M. Marzook, M. Reisjalali, M. Salvalaglio and C. Molteni, *Phys. Chem. Chem. Phys.*, 2022, **24**, 12476–12487.

26 A. Mohandesi and P. G. Kusalik, *J. Cryst. Grow.*, 2018, **483**, 156–163.

27 R. L. Walker, K. Searles, J. A. Willard and R. R. H. Michelsen, *J. Chem. Phys.*, 2013, **139**, 244703.

28 Y. Uda, S. Zepeda, F. Kaneko, Y. Matsuura and Y. Furukawa, *J. Phys. Chem. B*, 2007, **111**, 14355–14361.

29 J. F. D. Liljeblad, I. Furó and E. C. Tyrode, *Phys. Chem. Chem. Phys.*, 2017, **19**, 305–317.

30 O. Sterner, C. Karageorgaki, M. Zürcher, S. Zürcher, C. W. Scales, Z. Fadli, N. D. Spencer and S. G. P. Tosatti, *ACS Appl. Mater. Interfaces*, 2017, **9**, 20150–20160.

31 I. Tagliaro, V. Radice, R. Nisticò and C. Antonini, *Colloids Surf., A*, 2024, **700**, 134695.

32 M. H. M. A. Shibraen, H. Yagoub, X. Zhang, J. Xu and S. Yang, *Appl. Surf. Sci.*, 2016, **370**, 1–5.

33 Y. Cheng, X. Zhang, J. Zhang, Z. He, Y. Wang, J. Wang and J. Zhang, *Chem. Eng. J.*, 2022, **441**, 136016.

34 J. Chen, Z. Luo, Q. Fan, J. Lv and J. Wang, *Small*, 2014, **10**, 4693–4699.

35 L. Stendardo, G. Gastaldo, M. Budinger, V. Pommier-Budinger, I. Tagliaro, P. F. Ibáñez-Ibáñez and C. Antonini, *Appl. Surf. Sci.*, 2023, **641**, 158462.

36 H. H. G. Jellinek, *Can. J. Phys.*, 1962, **40**, 1294–1309.

37 C. Ospina, P. F. Ibáñez-Ibáñez, I. Tagliaro, L. Stendardo, S. Tosatti and C. Antonini, *J. Colloid Interface Sci.*, 2025, **677**, 494–503.

38 B. N. J. Persson and E. C. Tyrode, *J. Chem. Phys.*, 2023, **158**, 234701.

39 H. Dosch, A. Lied and J. H. Bilgram, *Surf. Sci.*, 1995, **327**, 145–164.

40 A. Atila, S. V. Sukhomlinov and M. H. Müser, *Phys. Rev. Lett.*, 2025, **135**, 066204.

41 X. Cui, C. Yang, Q. Sun, W. Zhang and X. Wang, *Langmuir*, 2024, **40**, 14214–14223.

42 O. Sterner, M. Giazzon, S. Zürcher, S. Tosatti, M. Liley and N. D. Spencer, *ACS Appl. Mater. Interfaces*, 2014, **6**, 18683–18692.

43 Â. Serrano, O. Sterner, S. Mieszkin, S. Zürcher, S. Tosatti, M. E. Callow, J. A. Callow and N. D. Spencer, *Adv. Funct. Mater.*, 2013, **23**, 5706–5718.

44 R. Koguchi, K. Jankova and M. Tanaka, *Acta Biomater.*, 2022, **138**, 34–56.

45 S. Kumar, B. Mohan, C. Fu, V. Gupta and P. Ren, *Coord. Chem. Rev.*, 2023, **476**, 214876.

46 G. Abatangelo, V. Vindigni, G. Avruscio, L. Pandis and P. Brun, *Cells*, 2020, **9**, 1743.

47 P. Taweechat, R. B. Pandey and P. Sompornpisut, *Carbohydr. Res.*, 2020, **493**, 108026.

48 A. Almond, *Glycobiology*, 2003, **13**, 255–264.

49 F. Franks, *Water*, Royal Society of Chemistry, London, 1983.

50 E. Brini, C. J. Fennell, M. Fernandez-Serra, B. Hribar-Lee, M. Lukšič and K. A. Dill, *Chem. Rev.*, 2017, **117**, 12385–12414.

51 Q. Dong, X. Guo, L. Li, C. Yu, L. Nie, W. Tian, H. Zhang, S. Huang and H. Zang, *Sci. Rep.*, 2020, **10**, 1387.

52 E. Yu, S.-C. Kim, H. J. Lee, K. H. Oh and M.-W. Moon, *Sci. Rep.*, 2015, **5**, 9362.

53 M. Pedroni, E. Vassallo, M. Aloisio, M. Brasca, H. Chen, R. Donnini, G. Firpo, S. Morandi, S. M. Pietralunga, T. Silvetti, G. Speranza and T. Virgili, *Surf. Coat. Technol.*, 2023, **471**, 129828.

54 E. Vassallo, M. Pedroni, S. M. Pietralunga, R. Caniello, A. Cremona, F. Di Fonzo, F. Ghezzi, F. Inzoli, G. Monteleone, G. Nava, V. Spampinato, A. Tagliaferri, M. Zani and G. Angella, *Thin Solid Films*, 2016, **603**, 173–179.

55 J. H. Scofield, *J. Electron Spectrosc. Relat. Phenom.*, 1976, **8**, 129–137.